Available online at www.sciencedirect.com
SCIENCE DIRECT®
International Journal of Heat and Mass Transfer 49 (2006) 2972–2983
International Journal of HEAT and MASS TRANSFER
www.elsevier.com/locate/ijhmt

Non-gray radiative convective conductive modeling of a double glass window with a cavity filled with a mixture of absorbing gases

Kamal A.R. Ismail *, Carlos Salinas S.

Department of Thermal and Fluids Engineering – FEM – UNICAMP, P.O. Box 6122, CEP 13083-970, Campinas (SP), Brazil

Received 22 July 2005; received in revised form 20 January 2006
Available online 11 May 2006

Abstract

Coupled radiation and natural convection heat transfer occurs in vertical enclosures with walls at different temperatures filled with gas media. In glass window thermal insulation applications in hot climates, infrared absorbing gases appear as an alternative to improve their thermal performance. The thermal modeling of glass windows filled with non-gray absorbing gases is somewhat difficult due to the spectral variation of the absorption coefficients of the gases and the phenomena of natural convection. In this work, the cumulative wavenumber (CW) model is used to treat the spectral properties of mixtures of absorbing gases and the radiative transport equation is solved using CW model and the discrete ordinates method. Due to the range of temperature variation, the mixture of gases is considered as homogeneous. The absorption coefficients were obtained from the database HITRAN. First, the natural convection in a cavity with high aspect ratio is modeled using a CFD code and the local and global Nusselt numbers are computed and compared with available empirical correlations. Also, the flow pattern for different Rayleigh numbers is analyzed. Then, the heat transfer in the gas domain is approximated by a radiative conductive model with specified heat flux at boundaries which is equivalent to convective transport at the walls surroundings. The energy equation in its two-dimensional form is solved by the finite volume technique. Three types of gas mixtures, highly absorbing, medium and transparent are investigated, to determinate their effectiveness in reducing heat gain by the gas ambient. Reflective glasses are also considered. The numerical method to solve radiative heat transport equation in gray and non-gray participant media was validated previously. The temperatures distributions in the gas and the glass domain are computed and the thermal performance of the gas mixtures is evaluated and discussed. Also, comparison with pure radiative conductive model is shown.
© 2006 Elsevier Ltd. All rights reserved.

Keywords: Numerical modeling; Cumulative wavenumber model; Radiation conduction convection; Glazing; Non-gray gases

1. Introduction

Convection heat transfer in gas layers within rectangular cavities appears in many engineering applications and hence a great deal of investigations were dedicated to better understanding of the problem [1–4]. Many experimental results and correlations can be found in Wright [2].

In tropical climates of the southern hemisphere the principal advantage of a thermal glass window is to avoid heat transfer to the internal ambient and consequently reduce the cooling load requirements to maintain thermal comfort. In the interior of a building, direct sunlight is the source of significant visibility and directs up to 800 W/m^2 of radiation through windows into the building interior. The use of selective films allows changes in both solar and infrared transmittance, reflectance and absorptance of glass windows. The films can be designed to absorb or reflect according to the wavelength of the incident radiation and generally can be incorporated with glass window filling gases. Other techniques employ low conductivity gases such as Argon and Helium instead of air as a filling gas in double glass windows. Double glass windows filled with infrared absorbing gases, ventilated double glass windows, and glass windows employing combination of these

* Corresponding author. Tel.: +55 19 37883214; fax: +55 19 37883213.
E-mail addresses: kamal@fem.unicamp.br (K.A.R. Ismail), csalinas_99@yahoo.com (C. Salinas S.).

0017-9310/$ - see front matter © 2006 Elsevier Ltd. All rights reserved.
doi:10.1016/j.ijheatmasstransfer.2006.01.051

Nomenclature

A	area
C_η	absorption cross-section (cm^2/molecule)
C_j	supplementary cross-section (cm^2/molecule)
c_p	specific heat
D_{ij}	fractional gray gas
$f_{wi,j}$	weight factor of CW model, Eq. (35)
F	solar heat gain coefficient
h	convective coefficient
H	height
H_j	sum of spectral subintervals
k	thermal conductivity
$\mathbf{I}$	radiation intensity
$\mathbf{I}_b$	blackbody radiation intensity
$\mathbf{J}$	fractional radiation intensity
$\mathbf{J}_b$	fractional blackbody radiation intensity
L	width of the air layer
M	number of discrete directions
$\mathbf{M_i}$	molecular weight
N	Planck number
N_c	molar density of the gas
Nu	Nusselt number
Pr	Prandtl Number
q	local heat flux per unit area
q_m	non-radiative heat flux
q_r	net total radiative flux
Ra	Rayleigh number
r_a	aspect ratio
Re	Reynolds number
s	distance along a given line if sight
$\mathbf{S}_{df}$	deferred factor correction
St	Stanton number
T	temperature
THG	total heat gain
u	velocity x-axis
v	velocity y-axis
$u_{i,j}(s)$	function location dependent Eq. (38)
V	volume
W	cumulative wavenumber function
$\mathbf{w}_m$	weight of angular quadrature
x/y	x/y-coordinate
y^+	dimensionless distance
Y	gas molar fraction

Greek symbols

α	absorptance
α_a	thermal diffusivity
β	extinction coefficient
β_a	coefficient of thermal expansion of air
ε	total emissivity
ν	kinematics viscosity
η	wavenumber
κ	absorption coefficient
ρ	reflectivity
ρ_a	density
σ	scatter coefficient
τ	transmittance
τ_w	wall shear stress
μ	direction cosine
ξ	direction cosine
$\upsilon_{i,j}(\eta)$	function wave number dependent Eq. (33)
Ω	direction vector along s
ϕ	fluid property
Δ	spectral interval

Subscripts

b	blackbody
E	of the control volume face east of the node (**i**, **j**), or wall quantity
h/c	hot/cold
i,j	spectral position
i, **j**	space grid position
n	number of species of a mixture
η	spectral dependence
g	number of gray gases
W	of the control volume face west of the node (**i**, **j**), or wall quantity

Superscripts

n	iteration number
m	the mth discrete ordinate
*	relative to reference point

techniques have been investigated. Extensive bibliography about thermal glazing types is found in the literature [5,6]. The use of gases with strong infrared radiation absorption characteristics was investigated and some simplified models for spectral radiation modeling was formulated [7,8]. Recently, one accurate model for spectral radiation modeling was applied to modeling horizontal double glass window [9]. Based upon results for night time conditions in terms of the total heat gain it was concluded that the infrared radiation absorbing gases have a small impact in reducing heat transfer across thermal windows [7–9]. Muneer et al. [10] presented a model to handle the combined modes of conduction, convection and radiation in a glass window filled with non-participant gas and determined the glass temperature at the bottom of the window. Due to the increasing interest in applying the spectral integration of radiative transport equation in practical applications, several real gas models were developed [11–13].

In the present work, the CW model [14] is adopted. This model needs the cumulative wavenumber function of

distribution to treat the spectral variation of the absorption coefficients of the absorbing gases. The methods to construct and use this distribution function are outlined in [14,15]. In this work, the spectral properties of the gases are obtained from Hitran and Hitemp [16]. One main objective of the present study is to use a general method to approximate the spectral solution of the combined radiation and natural convection heat transfer in mixtures of non-gray gases, in vertical rectangular cavity and apply the results to model a thermal glass window filled with infrared absorbing gases.

2. Natural convection analysis

In most practical problems of convective transport to or from a rigid surface, the flow in the vicinity of the body is in turbulent motion. However, at the solid–fluid interface itself, the no-slip boundary condition ensures that turbulent velocity fluctuations vanish. Thus, at the wall, diffusive transport of heat and momentum in the fluid is precisely expressible by the laws applicable to laminar flow. There is a thin but very important sub-layer immediately adjacent to the solid surface where the transport of heat and momentum is predominant by molecular diffusion.

In the first part of this paper, the model for natural convection induced flow in vertical cavities of high aspect ratio is presented. This type of cavities is present in double glass windows filled with mixture of radiation absorbing gases. Geometry of cavity is shown in Fig. 1. The mean Nusselt number (Nu) which represent the non-radiative heat (q_m) which includes conduction and convection through a gas layer can be written as

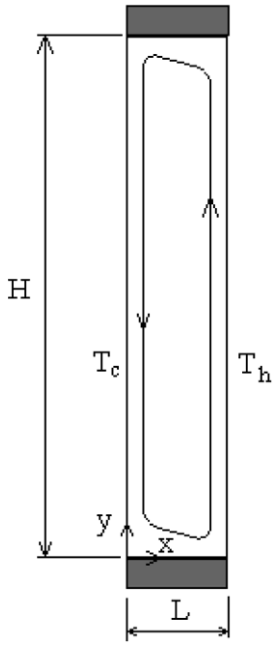

Fig. 1. Cavity filled with air, isothermal vertical walls with specified temperatures and adiabatic horizontal walls.

$$Nu = \frac{q_m L}{k(T_h - T_c)} \tag{1}$$

where k (W m^{-1} K^{-1}) is the thermal conductivity of air at T_m; L (m) is the width of the air layer; q_m (W m^{-2}) is the mean non-radiative heat flux through the air layer; T_c (K) is the temperature of the cold wall; T_h is the temperature of the hot wall and T_m is the temperature at which the air properties are estimated, $T_m = (T_h + T_c)/2$.

For the case of vertical cavities, it is well established that the Nusselt number depends upon the Rayleigh and Prandtl number (Ra_L, Pr) as well as the aspect ratio (r_a), i.e. $Nu = f(Ra_L, Pr, r_a)$, where

$$Ra_L = \frac{gL^3\beta_a(T_h - T_c)}{\alpha_a \nu} \quad \text{and} \quad r_a = \frac{H}{L} \tag{2}$$

where α_a (m^2 s^{-1}) is the air thermal diffusivity at T_m; g (m s^{-2}) is the gravity acceleration; β_a (K^{-1}) is the coefficient of thermal expansion of air and ν (m^2 s^{-1}) is the kinematics viscosity of the air at T_m. The Prandtl number of the air at 20 °C is 0.71 while the Prandtl number for the filling gases is around the same value, for instance Prandtl number for Argon is 0.68, krypton is 0.65, xenon is 0.66 and SF6 is 0.68. Hence it is possible to write Nu as function of only Ra_L and r_a.

In modeling the flow field all the thermophysical properties are considered constant except the density which is treated by using the Boussinesq approximation. The flow in this case is considered steady and two-dimensional. In this work, to quantify the heat transfer due to natural convection, numerical simulations were realized to solve the equation of energy and the equation of momentum using the CFD Phoenics code. The boundary conditions are stated as follows:

Temperature field:

$$T(x=0,y) = T_c; \quad T(x=L,y) = T_h;$$
$$\left.\frac{\partial T}{\partial y}\right|_{y=0} = 0; \quad \left.\frac{\partial T}{\partial y}\right|_{y=H} = 0 \tag{3}$$

Momentum equations:

$$u(x=0,y) = v(x=0,y) = 0; \quad u(x=L,y) = v(x=L,y) = 0;$$
$$u(x,y=0) = v(x,y=0) = 0; \quad u(x,y=H) = v(x,y=H) = 0 \tag{4}$$

The simulations were realized for $r_a = 40$ and Rayleigh number from 10^3 to 10^5. $T_m = 20$ °C for all simulations while $H = 1.2$ m and the temperature difference between the hot and cold walls varied from 2.0 to 39 °C. The local heat flux per unit area q, is related to the Stanton number St [17]:

$$St = \frac{q}{\rho_a v c_p (T - T_w)} \tag{5}$$

where ρ_a (kg m^{-3}) is the air density; c_p (J kg^{-1} K^{-1}) is the air specific heat; T (°C) is the temperature of the control volume near to wall; and T_w (°C) is the wall surface temperature. The heat transfer coefficient in the wall can be calculated from

$$h = St \times \rho v c_p \tag{6}$$

The numerical solutions were realized for the cases of both laminar and turbulent flow. For laminar flow the wall logarithmic law is adopted and for turbulent case the generalized law of wall logarithmic functions is used.

For the laminar flow case (the dimensionless distance from the wall $y^+ \leqslant 11.5$)

$$St = \frac{1}{Re \times Pr} \quad \text{or} \quad \left(q = \frac{k}{y^+}(T - T_w)\right) \tag{7}$$

where y^+ is given by

$$y^+ = \frac{u_\tau y \rho_a}{\mu} \tag{8}$$

and u_τ (m s^{-1}) is the friction velocity; $u_\tau = \left(\frac{\tau_w}{\rho_a}\right)^{0.5}$, where τ_w (N m^{-2}) is the wall shear stress.

For the turbulent flow case ($y^+ \geqslant 11.5$), the Stanton number is calculated by

$$St = \frac{\tau_w/(\rho_a u^2)}{0.9(1 + [\tau_w/(\rho_a u^2)])^{0.5} P} \tag{9}$$

where 0.9 is the turbulent Prandtl number and P is the Jayatilleke function

$$P = 9\left(\frac{Pr}{0.9} - 1\right)\left(\frac{0.9}{Pr}\right)^{0.25} \tag{10}$$

St and q were deduced from calculated values of u and τ_w.

The laminar and turbulent flows are modeled by using the turbulent models KCHEM-LOWRE, KEMODL-LOWRE and the standard K–E model. The computational grid used is 10×150 non-uniform having a variation factor of the geometrical progression along x-axis and power law along the y-axis. The model and numerical procedure used are validated by comparing the mean Nusselt number obtained with the following correlations:

Yin et al. [3]

$$Nu = 0.23 r_a^{-0.131} Ra_L^{0.269};$$
$$10^3 \leqslant Ra_L \leqslant 5 \times 10^6 \text{ and } 4.9 \leqslant r_a \leqslant 78.7 \tag{11}$$

Wright [2], $r_a \geqslant 40$

$$Nu = 0.0673838 Ra_L^{0.3}; \quad 5 \times 10^4 < Ra_L \leqslant 10^6 \tag{12a}$$

$$Nu = 0.028154 Ra_L^{0.4134}; \quad 10^4 < Ra_L \leqslant 5 \times 10^4 \tag{12b}$$

$$Nu = 1 + 1.75967 \times 10^{-10} Ra_L^{2.29847553}; \quad Ra_L \leqslant 10^4 \tag{12c}$$

EM 673 [4]

$$Nu = \text{Max}(0.035 Ra_L^{0.38}, 1) \tag{13}$$

Fig. 2 shows the computational results for a cavity of aspect ratio $r_a = 40$, $L = 0.03$ m, $H = 1.2$ m for the values of Rayleigh number in the laminar, transition and turbulent regimes. The results are in agreement with the correlations. Fig. 3a shows the isotherms for the same cases where the diffusive effects are dominant for Rayleigh number equals to 1084 and the convective effects are dominant for the case of Rayleigh number of 105,655. Fig. 3b shows the velocity profile for the same cases where one observe that the velocity profile is increased by the increase of the Rayleigh number and that the velocity profile is similar to the boundary layer profiles for high Rayleigh number. Except for Yin et al. work [3], the predicted values of Nusselt indicate about 20% deviation from correlations.

The Rayleigh number in double glass window with aspect ratio higher than 40 is in range of 20,000–40,000, where the diffusive effects are dominant at the middle of the gas layer while the convective effects are important close to the solid walls. To include the effects of natural convection in modeling double glass window, one can use radiative conductive model in the gas domain with specified heat flux at the vertical boundaries. This heat flux calculated by empirical correlations Wright [2], is specified at the center of the cell

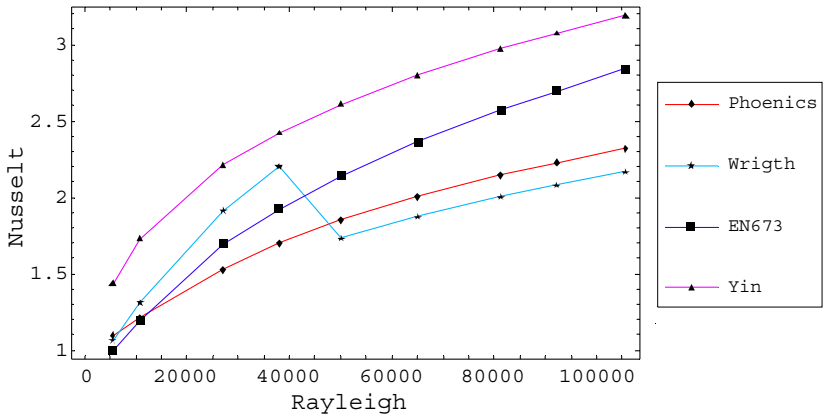

Fig. 2. Comparison of the values of $Nu = f(Ra_L, r_a)$ computed from empirical correlations with values of numerical solution.

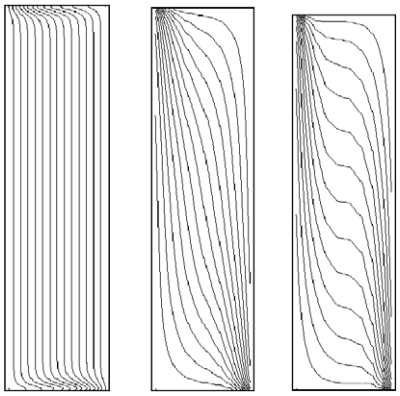

Fig. 3a. Isotherms for Rayleigh number equal to 1084, 27,094 and 105,665.

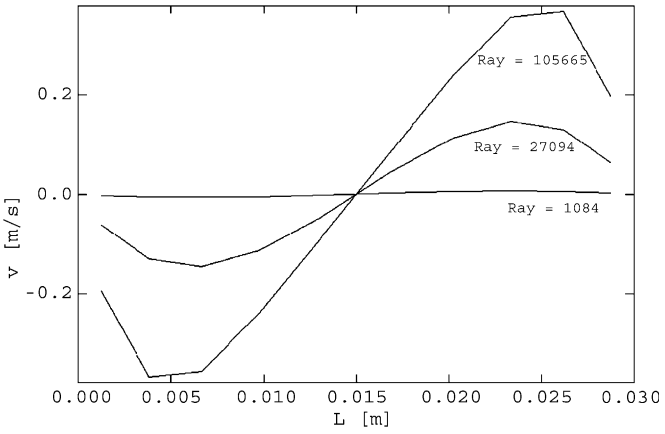

Fig. 3b. Velocity profile at $H/2$ for Ra_L equal to 1084, 27,094 and 105,665.

adjacent to the vertical walls. This is done in order to avoid including the conduction in the gas twice.

3. Non-gray formulation

3.1. The energy equation

The energy equation for the coupled radiation conduction heat transfer in an absorbing, emitting and isotropic scattering media in steady state with constant conductivity is written as [18]

$$k\nabla^2 T - \nabla \cdot q_r = 0 \tag{14}$$

where $\nabla \cdot q_r$, the divergence of the radiant flux vector q_r is one radiative source term.

3.2. The radiative transport equation (RTE) in gray media

The radiative transport equation for an absorbing, emitting gray gas with isotropic scattering can be written as [18],

$$(\Omega \cdot \nabla)\mathbf{I}(\mathbf{r},\Omega) = -(\kappa+\sigma)\mathbf{I}(\mathbf{r},\Omega) + \frac{\sigma}{4\pi}\int_{4\pi}\mathbf{I}(\mathbf{r},\Omega')\,d\Omega' + \kappa\mathbf{I}_b(\mathbf{r}) \tag{15}$$

where $\mathbf{I}(\mathbf{r},\Omega)$ is the radiation intensity in $\mathbf{r}$, and in the direction Ω; $\mathbf{I}_b(\mathbf{r})$ is the radiation intensity of the blackbody in the position $\mathbf{r}$ and at the temperature of the medium; κ is the gray medium absorption coefficient; σ is the gray medium scatter coefficient; and the integration is in the incident direction Ω'.

For diffusely reflecting surfaces the radiative boundary condition for Eq. (15) is

$$\mathbf{I}(\mathbf{r},\Omega) = \varepsilon\mathbf{I}_b(\mathbf{r}) + \frac{\rho}{\pi}\int_{\mathbf{n}\cdot\Omega'<0}|\mathbf{n}\cdot\Omega'|\mathbf{I}(r,\Omega')\,d\Omega' \tag{16}$$

where $\mathbf{r}$ lies on the boundary surface Γ, and Eq. (16) is valid for $\mathbf{n}\cdot\Omega > 0$. $\mathbf{I}(\mathbf{r},\Omega)$ is the radiation intensity leaving the surface at the boundary condition, ε is the surface emissivity, ρ is the surface reflectivity and $\mathbf{n}$ is the unit vector normal to the boundary surface. In the method of discrete ordinates, the equation of radiation transport is substituted by a set of M discrete equations for a finite number of directions Ω_m, and each integral is substituted by a quadrature series [19],

$$(\Omega_m \cdot \nabla)\mathbf{I}(\mathbf{r},\Omega_m) = -\beta\mathbf{I}(\mathbf{r},\Omega_m) + \frac{\sigma}{4\pi}\sum_{m=1}^{M}\mathbf{w}_m\mathbf{I}(\mathbf{r},\Omega_m) + \kappa\mathbf{I}_b(\mathbf{r}) \tag{17}$$

This angular approximation transforms the original equation into a set of coupled differential equations, with $\beta = (\kappa+\sigma)$ as the extinction coefficient.

$$S_m = \frac{\sigma}{4\pi}\sum_{m=1}^{M}\mathbf{w}_m\mathbf{I}(\mathbf{r},\Omega_m) \tag{18}$$

where S_m represents the entering scattering source term.

The local divergence of the radiative flux is related to the local intensities by

$$\nabla \cdot q_r = \kappa\left[4\pi\mathbf{I}_b(\mathbf{r}) - \int_{\Omega=4\pi}\mathbf{I}(\mathbf{r},\Omega')\,d\Omega'\right] \tag{19}$$

Eq. (19) in discrete ordinates can be written as

$$\nabla \cdot q_r = 4\pi\kappa\mathbf{I}_b(\mathbf{r}) - \sum_{m=1}^{M}\mathbf{w}_m\kappa\mathbf{I}_m \tag{20}$$

where $\mathbf{w}_m$ are the ordinates weight, M is the number of directions Ω_m of the angular quadrature and $\mathbf{I}_m$ is obtained by solving the radiative transport equation in discrete ordinates.

3.3. The RTE in the cumulative wavenumber model

The radiative transport in an absorbing and emitting medium along a trajectory S in the direction Ω in spectral form is given by [18]

$$\frac{\partial \mathbf{I}_\eta}{\partial s} = -\kappa_\eta \mathbf{I}_\eta + \kappa_\eta \mathbf{I}_{b\eta} \tag{21}$$

In the CW model [14], the total range of the absorption cross-section $C\eta$ is subdivided into supplementary absorption cross-section of gray gases C_j, $j = 1,\ldots,n$, where n is the number of gray gases. The intersection of the two spectral subdivisions is used to define the modeling of the fractional gray gas D_{ij} and the sum of the fractional gray gases establishes the complete range of number of wave.

In CW model [14] Eq. (21) is written as

$$\frac{\partial \mathbf{J}_{i,j}}{\partial s} = -\kappa_j \mathbf{J}_{i,j} + \kappa_j \mathbf{J}_{bi,j} \tag{22}$$

where $\mathbf{J}_{i,j}$ is the intensity of the fractional gray gas D_{ij} and κ_j is the absorption coefficient of gray gas determined by the equation

$$\kappa_j = N_c \sqrt{C_j C_{j-1}} \tag{23}$$

where N_c is the molar density of the gas (molecules/cm^3).

The term $\mathbf{J}_{bi,j}$ in Eq. (22) is the source radiative term at the black body fractional intensity

$$\begin{aligned}\mathbf{J}_{bi,j}(s) &= \int_{\Delta i} \mathbf{I}_{b\eta}(T(s),\eta)\,\mathrm{d}[\upsilon_{ij}(s)] \\ &= \int_{\Delta i} \mathbf{I}_{b\eta}(T(s),\eta)\,\mathrm{d}[W(C_j,s^*,\eta) - W(C_{j-1},s^*,\eta)]\end{aligned} \tag{24}$$

where $W(C_j,s,\eta)$ is the cumulative wavenumber function as defined by Solovjov and Webb [14] and s^* is one spatial reference point where gas properties are known. The term $\mathbf{I}_{b\eta}(T(s),\eta)$ is the black body spectral intensity.

Eq. (24) can be rewritten as

$$\mathbf{J}_{bi,j}(s) = \frac{(W(C_j,s^*,\eta_i) - W(C_j,s^*,\eta_{i-1})) - (W(C_j,s^*,\eta_i) - W(C_j,s^*,\eta_{i-1}))}{\eta_i - \eta_{i-1}} \times \int_{\eta_{i-1}}^{\eta_i} \mathbf{I}_{b\eta}(T(s),\eta)\,\mathrm{d}\eta \tag{25}$$

and

$$f_{wi,j} = \frac{(W(C_j,s^*,\eta_i) - W(C_j,s^*,\eta_{i-1})) - (W(C_j,s^*,\eta_i) - W(C_j,s^*,\eta_{i-1}))}{\eta_i - \eta_{i-1}} \tag{26}$$

The Planck function is determined as the sum of the $\mathbf{J}_{bi,j}(s)$ for all the fractional gray gases. The boundary condition for non-gray walls, diffusively emitting and reflecting is

$$\mathbf{I}_\eta(s_w,\widehat{\Omega}) = \varepsilon_{\eta w}\mathbf{I}_{b\eta}(T_w) + \frac{\rho_{\eta w}}{\pi}\int_{\mathbf{n}\cdot\widehat{\Omega}'<0} \mathbf{I}_\eta(s_w,\widehat{\Omega}')|\mathbf{n}\cdot\widehat{\Omega}'|\,\mathrm{d}\widehat{\Omega}' \tag{27}$$

where s_w define the point on the frontier surface and the subscript w refers to the quantity evaluated at the frontiers. $\varepsilon_{\eta w}$ is the spectral emissivity and $\rho_{\eta w}$ is the spectral reflectivity of the frontier. Integration of Eq. (36) yields

$$\mathbf{J}_{i,j}(s_w,\widehat{\Omega}) = \varepsilon_{iw}\mathbf{J}_{bi,j}(T_w) + \frac{\rho_{iw}}{\pi}\int_{\mathbf{n}\cdot\widehat{\Omega}'<0} \mathbf{J}_{i,j}(s_w,\widehat{\Omega}')|\mathbf{n}\cdot\widehat{\Omega}'|\,\mathrm{d}\widehat{\Omega}' \tag{28}$$

When the equation of radiative transport, Eq. (22) together with the boundary conditions Eq. (28) are solved for all the fractional gray gases $\mathbf{J}_{i,j}$, the total radiation intensity is determined from the sum of all intensities of gases with the correction factor $u_{i,j}(s)$ as weight [14].

$$\mathbf{I}(s) = \int_0^\infty \mathbf{I}_\eta(s)\,\mathrm{d}\eta = \sum_{i,j} u_{i,j}(s)\mathbf{J}_{i,j}(s) \tag{29}$$

For the case of isothermal and homogeneous media, $u_{i,j}(s) = 1$

For a mixture of (g) gases of molar density N_c, the function $u_{i,j}(s)$ is defined as [14]

$$u_{i,j}(s) = \frac{\sum_g \left[W_g(C_j/Y_g) - W_g(C_{j-1}/Y_g)\right]}{\sum_g \left[W_g(C_j/Y_g) - W_g(C_{j-1}/Y_g)\right]} \tag{30}$$

where Y_g is the molar fraction of gas species.

The radiative source term for the gray gas j is determined from equation

$$\nabla\cdot q_{r,j} = 4\pi\kappa_j\sum_i \mathbf{J}_{bi,j} - \sum_{m=1}^{M}\mathbf{w}_m\kappa_j\mathbf{I}_m \tag{31}$$

and the total source term is written as

$$\nabla\cdot q_r = \sum_j \nabla\cdot q_{r,j} \tag{32}$$

To discretize the spectral radiative transport equation in 2D using the CW model in every fractional gray gas (i,j), one can write Eq. (22) based upon the method outlined by Ismail and Salinas [20], as,

$$(\mathbf{J}^{\mathbf{m}}_{\mathbf{i},\mathbf{j}})^{n+1} = \frac{V_{\mathbf{i},\mathbf{j}}(\kappa\mathbf{J}_{\mathbf{bi},\mathbf{j}})^n + |\mu_m|A_x(\mathbf{J}^{\mathbf{m}}_{\mathbf{i}-\frac{1}{2},\mathbf{j}})^{n+1} + |\xi_m|A_y(\mathbf{J}^{\mathbf{m}}_{\mathbf{i},\mathbf{j}-\frac{1}{2}})^{n+1} + \mathbf{S}^n_{df}}{|\mu_m|A_x + |\xi_m|A_y + \kappa V_{\mathbf{i},\mathbf{j}}} \tag{33}$$

where

$$\mathbf{S}^n_{df} = |\mu_m|A_x(\mathbf{I}^{\mathbf{m}}_{\mathbf{i},\mathbf{j}} - \mathbf{I}^{\mathbf{m}}_{\mathbf{i}+\frac{1}{2},\mathbf{j}})^n + |\xi_m|A_y(\mathbf{I}^{\mathbf{m}}_{\mathbf{i},\mathbf{j}} - \mathbf{I}^{\mathbf{m}}_{\mathbf{i},\mathbf{j}+\frac{1}{2}})^n \tag{34}$$

$\mathbf{S}^n_{df}$ is the deferred correction term in nth iteration. Here, the spectral domain subscripts (i,j) are omitted and the space domain subscripts are $(\mathbf{i},\mathbf{j})$, $\mathbf{m}$ indicate the mth direction of the angular quadrature, A is the area and V the volume of control volume $(\mathbf{i},\mathbf{j})$.

The values of the fluxes in the faces $(\mathbf{J}^{\mathbf{m}}_{\mathbf{i}+\frac{1}{2},\mathbf{j}})^n$ and $(\mathbf{J}^{\mathbf{m}}_{\mathbf{i},\mathbf{j}+\frac{1}{2}})^n$ are interpolated using the CLAM or the genuinely multidimensional (GM) scheme [20], while the values of the fluxes $(\mathbf{J}^{\mathbf{m}}_{\mathbf{i}-\frac{1}{2},\mathbf{j}})^{n+1}$ and $(\mathbf{J}^{\mathbf{m}}_{\mathbf{i},\mathbf{j}-\frac{1}{2}})^{n+1}$ are interpolated using a step scheme. Several numerical experiments were realized to ensure that the algorithm does not have any directional march error and also to determine an adequate value for the over-relaxation factor.

3.4. Validation

To validate the method of solution of the radiative transport equation it is proposed to solve the radiative heat

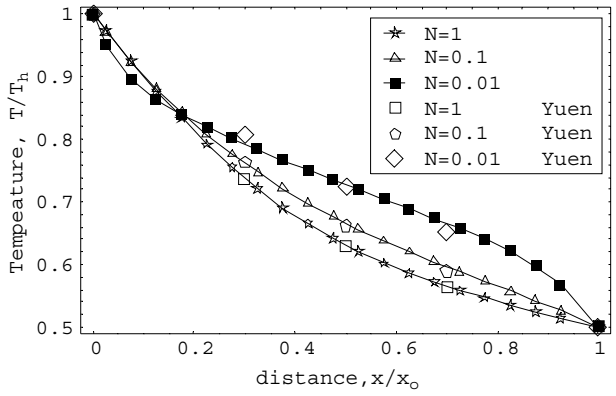

Fig. 4. Temperature distribution for different N values 2D radiation–conduction heat transfer in gray media solution.

transfer in a square cavity with a gray participant media where the cavity have three black cold walls and one hot black wall, the medium is cold and emitter with $\beta = 1$, as in [21]. Different quadratures are tested to evaluate the accuracy of the solution. Also the CLAM and GM spatial schemes [20] were tested and compared with the exact solution [21]. For brevity results is presented here and can be found in previous work [20]. Additional conduction radiation validation tests were realized for the case presented in [22], composed of a square cavity with three cold walls at temperature T_c and one hot wall at temperature T_h, where $T_h = 2T_c$. The evaluation of the accuracy of different angular quadratures used was done by comparison with available results in the literature [22]. The LC11 quadrature [23], with 48 ordinates has the same accuracy as that Tn6 quadrature with 144 ordinates in two-dimensional space. All results shown here is with LC11 quadrature. Fig. 4 shows the predicted temperature distribution for different N compared with the results of [22]. The CW real gas model and the numerical algorithm are validated by comparison with the results of the one-dimension test case presented in [14], where the medium in this case is a homogeneous isothermal mixture of combustion gases at 1000 K and 1 atm total pressure occupying a space of 1 m width between two parallel plates. The molar fractions of H_2O, CO_2 and CO in the mixture are 0.2, 0.1 and 0.03, respectively and the rest is nitrogen. The comparative results are not shown here by brevity and can be found in previous work [15].

4. Modeling of double glass window

To investigate the viability of using infrared absorbing gases to improve the thermal efficiency of vertical glass windows exposed to solar radiation in hot climate, three mixtures of gases are used, the first is a strongly absorbing gas mixture composed of HFC-32, HFC-134a, HFC-143a and SF6 in equal parts. The second mixture has intermediate absorbing characteristics and is composed of CFC-12, CFC-13, CFC-14 and SF6 in equal parts based upon the estimates in [7]. The third mixture is transparent to infrared radiation, in this case air is used. The cumulative wavenumber function for each gas at its molar fraction is used to calculate the factor $f_{wi,j}$ in Eq. (26).

4.1. Geometry and energy balance

Consider a vertical double glass window heated from outdoor by solar irradiation formed by two parallel glass sheets of 0.006 m thickness and 1 m × 1 m of area, separated by a distance which can be varied from 0.008 m to 0.040 m filled with a mixture of participant non-gray gases and the whole system is in steady state, that is, all the radiation absorbed by the gas is re-emitted. The external and internal ambient temperatures are 35 °C and 24 °C, respectively. The indoor and outdoor convective coefficients are 8.3 and 16.7 W/m K, respectively. The temperatures of the external and internal glass sheets can be determined from an energy balance for each glass sheet by considering radiation and convection heat transfer with the internal and external ambient, heat transfer by natural convection and radiation with the gas mixture in the cavity, and by radiation between the glass sheets in the spectral range where the gases are transparent to infrared radiation. The incident solar radiation is assumed constant at 600 W/m^2. Since the glass properties are nearly constant over the infrared spectrum, one may assume average values for the glass properties and also that the glass sheets are gray and reflective. In the present study two cases are examined, (1) window with two clear sheets, and (2) window with one external absorbing glass having a reflective coat at position 1 and one internal glass with low-E coating at position 3. Positions 2 and 4 are not coated. The solar absorptance (α_1) of surface 1 is varied from 0.35 to 0.55 while the solar reflectance (ρ_1) is kept as 0.16 [2]. The infrared transmittance of clear and absorbing glass is zero [5]. The emissivity of the clear glass (position 2 and 4) is 0.88 and the low-E coated glass (position 3) is 0.12 [5]. The glass thermal conductivity is 1.0 W/m K while the thermal conductivity of the gas mixture is calculated as a weight average of its molar fractions.

Fig. 5 shows a simplified energy balance of the glass window where Q_{wgas} and Q_{egas} are the incident gas radiative heat fluxes on the W and E faces; Q_{rvw} and Q_{rve} are the radiative heat fluxes in the transparent range leaving the W and E faces; Q_{cwg} and Q_{ceg} are the convective heat fluxes between the W and E faces and the gas; Q_{evw} and Q_{eve} are the radiative heat fluxes emitted by the faces W and E; Q_{solar} is the solar radiation incident over the external face of the glass W; Q_{cve} and Q_{cvi} are the convective heat fluxes between the glass sheets W and E and the external and internal ambient, respectively; Q_{re} and Q_{ri} are the radiation heat fluxes between the glass sheets W and E and the external and internal ambient, while e_W and e_E are the emissivities of the W and E faces, respectively. H is the window length and is considered as 1.0 m and unit width. The top and bottom extremities of the glass sheets are assumed

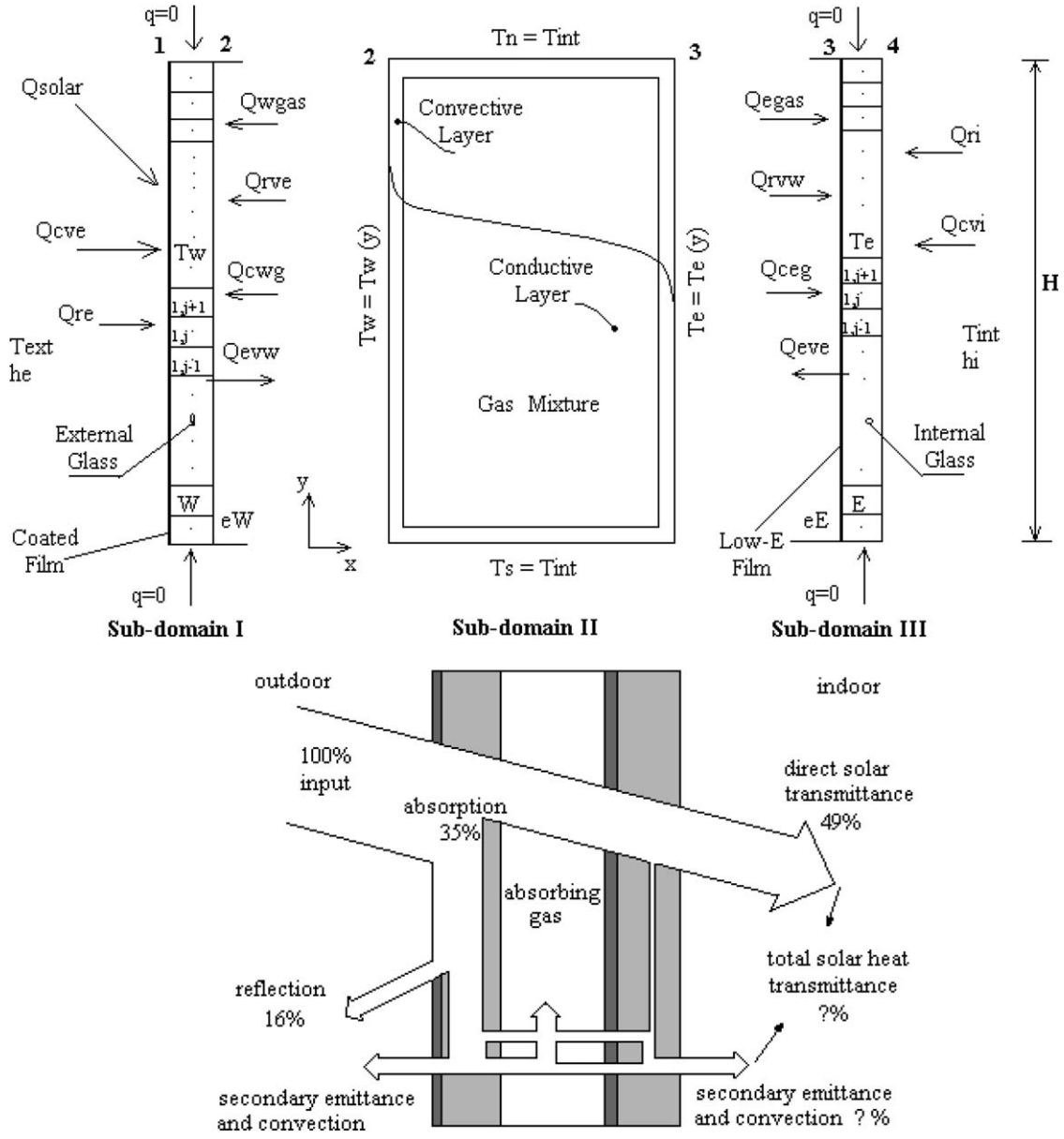

Fig. 5. Thermal window scheme – energy balance.

thermally insulated and at the temperature of the internal ambient.

All the thermo-physical properties are assumed constant and calculated at the mean temperature of the gas mixture except the density which is calculated at the local temperature. The properties of the gas mixture are calculated considering that it is composed of ideal gases and hence the density of the mixture is calculated from

$$\rho_m = \rho_i \frac{\sum_i^n y_i M_i}{M_i} \tag{35}$$

where y_i is the molar fraction of element i; M_i is the molar weight of element i; n is number of elements; ρ_i is density of element i; ρ_m is density of the mixture.

In case of calculating other properties such as thermal conductivity, viscosity, specific heat, etc., one can use

$$\phi = (\phi_1 + \phi_2 + \cdots + \phi_n)/n \tag{36}$$

where ϕ is the property under consideration.

The temperatures of the glass sheets are calculated iteratively from energy balances on each sheet. The total heat gain (THG) or the total solar heat transmittance is the heat passing over to the internal ambient by convection and radiation in addition to the total incident solar radiation which reaches the internal ambient.

$$\mathrm{THG} = \frac{1}{A_\mathrm{T}} \sum_j^{ny} h_i A_j (T_{\mathrm{E},j} - T_i) + \sigma \varepsilon_{\mathrm{E},j} A_j (T_{\mathrm{E},j}^4 - T_i^4) + \tau A_j Q_{\mathrm{solar}} \tag{37}$$

where τ is the coefficient of solar transmittance of the window, and is approximated by $\tau = 1 - \alpha_1 - \rho_1$. The solar heat gain coefficient F is calculated from:

$$F = \frac{\mathrm{THG}}{Q_{\mathrm{solar}}} \tag{38}$$

4.2. Method of calculation

The whole domain is sub-divided into three sub-domains as shown in Fig. 5 and energy balances are solved by iteration. The radiative energy transfer between the glass sheets and the absorbing gas mixture can be divided into two parts. In the first part, the gas mixture is acting as a participant medium while in the second part the mixture is transparent to infrared radiation. In the transparent part, a very small value of the gas absorption cross-section was adopted, $\kappa = 1 \times 10^{-30}\ \mathrm{cm^2/molecule}$, and hence one can approximate the radiation heat transfer between the glass sheets by the discrete ordinates method. The calculation of the radiation transfer in the transparent spectral range of the mixture is corrected in each iteration by considering the new values of the internal and external glass temperatures. In the spectral range where the gas is participant, the CW model combined with the DOM is used to solve the radiative transport equation using 20 gray gases. In the gas domain, the condition of convective heat flux at the center of the cells adjacent to the vertical walls (side 2 and 3) is imposed. The coupled radiation conduction model is solved by using the finite volume technique for the rest of the cells.

The simulations is initiated by calculating the temperature distribution in the internal and external glass sheets considering zero radiation from the gas mixture. The heat transferred by convection is calculated considering that the glass sheet has the same temperature as the external and internal ambient. Having calculated the temperature distribution in the glass sheets, one can calculate the radiative source term, the temperature distribution in the gas and the heat flux incident over the internal faces of the glass due to the gas radiation and consequently the radiation portion in the transparent range of the gas. The heat transferred by convection is recalculated using an updated density value according to the new temperatures and hence calculate the temperature distribution in the glass sheets. Repeat the iterations until achieve errors less than 10^{-5}

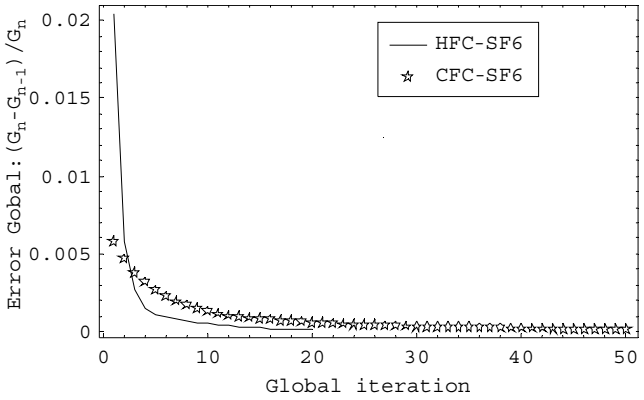

Fig. 6. Convergence error in glass temperature.

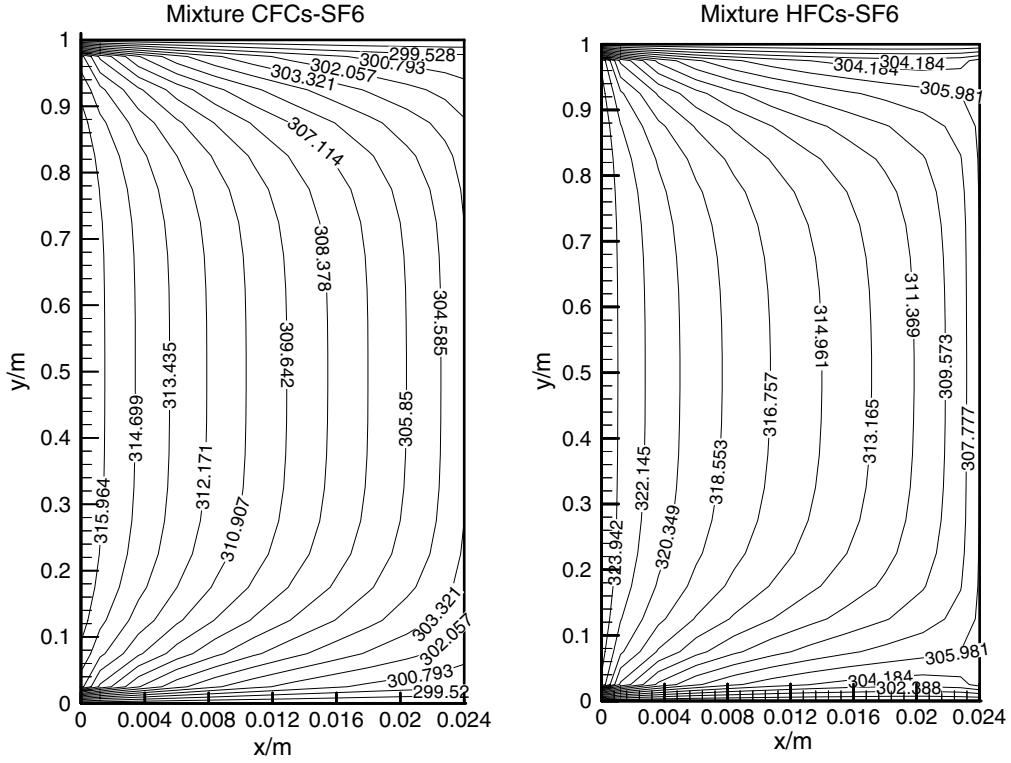

Fig. 7. Isotherms in mixture of gases CFC 12, 13, 14 and SF6, and HFC 22, 134a, 143a and SF6 for 0.024 m gap cavity.

for the temperatures of two consecutive iterations using the following relation

$$\text{error} = \text{Max}\left(\frac{T_j^n - T_j^{n-1}}{T_j^n}, p/j = 1, ny\right) < 10^{-5} \qquad (39)$$

where n is the number of iterations.

The convergence of the model and the results from the program is presented in Fig. 6 for the two absorbing mixtures. As can be verified the error is continuously decreasing with the increase of the number of iterations. To ensure the convergence of the solution of the energy equation, the authors used relaxation factors obtained experimentally. Also, the convergence of the inner and outer glass sheets temperatures was investigated and it was found that these temperatures converged smoothly.

5. Results and conclusion

Fig. 7 shows the isothermal contours in the CFC gas mixture and the HFC gas mixture filling the cavity under the same physical conditions. As can be observed the vertical temperature gradients in the central part of the gap are relatively small in comparison with the gradients near the top and bottom ends of external glass. Notice that the temperature profiles are not linear and that the gas temperature in the layers near the north and southern frontiers are affected by the imposed boundary conditions at the window top and bottom ends. Fig. 8 shows a comparison of the gas temperatures in the middle of the gas gap for different spacings between the glass sheets in a window of geometry as shown in Fig. 5. One can observe that the gas temperature is higher when the gas mixture is highly absorbing. This is because the gas absorbs the radiation emitted and reflected by the glass sheets and hence increase its temperature until achieving steady state. This indicates that highly absorbing gas mixtures are not effective in this case. The effect of the size of the gap between the glass sheets is also investigated and one can observe that the increase of the gap size leads to reducing the temperature of the internal glass, but the reduction is not significant. Figs. 9a and 9b show the temperature distribution along the vertical direction of the internal glass for the strong and intermediate absorbing mixtures for different gap sizes. One can observe that higher temperatures are achieved when the filling gas is a strong absorbing gas mixture. Fig. 10 shows a comparison of the predicted distribution of gas temperature in intermediate absorbing mixture for different gap size according to the present radiative convective conductive model and when using a purely radiative–conductive model. It is seen that radiative convective conductive model predicted smaller external glass temperature and higher internal glass temperature than radiative conductive model. This effect can be attributed to the convective transport.

Fig. 11 shows the temperature distribution in a highly absorbing gas mixture and the internal and external glass sheet temperatures for different values of external glass absorptance. It is interesting to observe that the temperature increases in the case of high absorbing glass sheets. The coefficient of total heat gain F for $\alpha = 0.35$, is presented in Table 1a in terms of the gap size for three gas mixtures and for a double glass window of clear glass

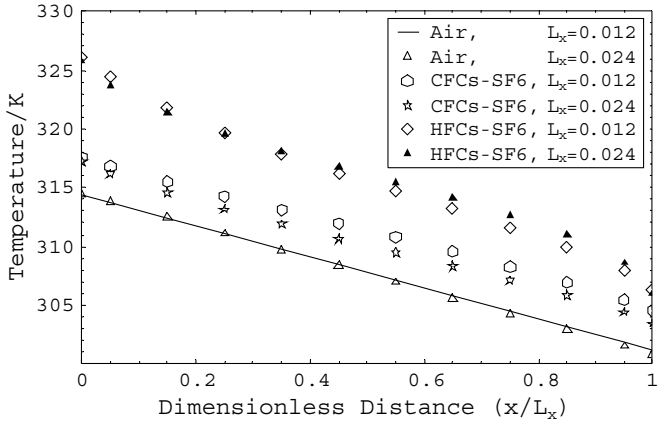

Fig. 8. Comparison of gas temperature distribution at middle cross-section of glazing with absorbing glass.

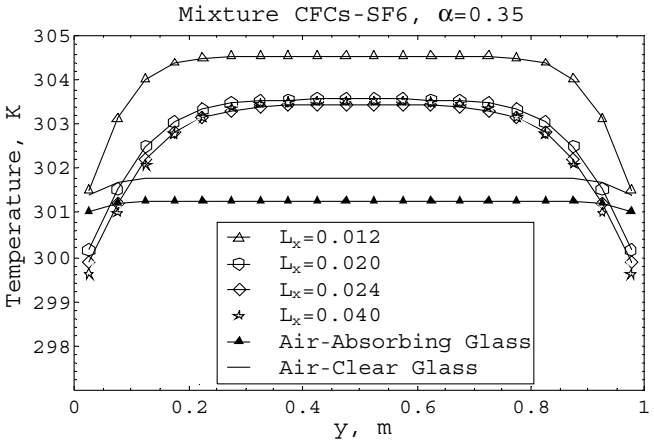

Fig. 9a. Comparison of the inner glass temperature distribution for different spacing between glass sheets for medium absorbing gas mixture.

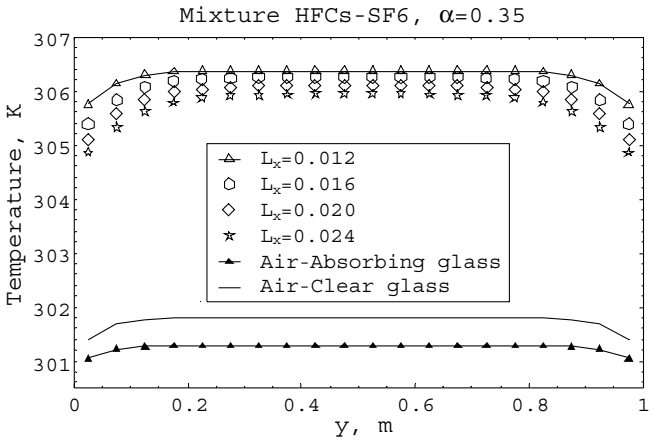

Fig. 9b. Comparison of the inner glass temperature distribution for different spacing between glass sheets for strong absorbing gas mixture.

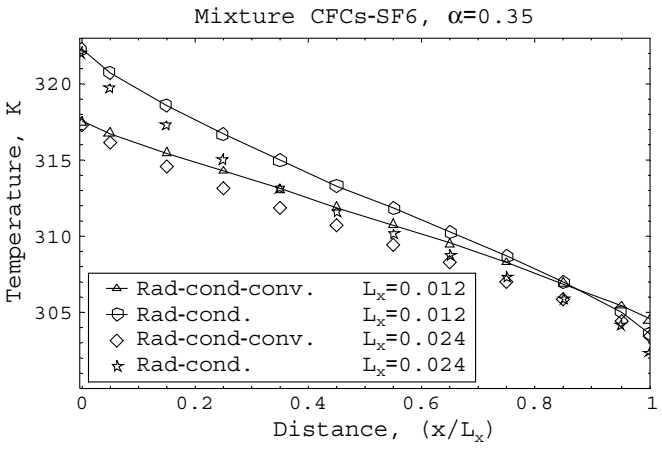

Fig. 10. Comparison of the gas temperature distribution for the radiation conduction convection modeling and the radiation conduction model.

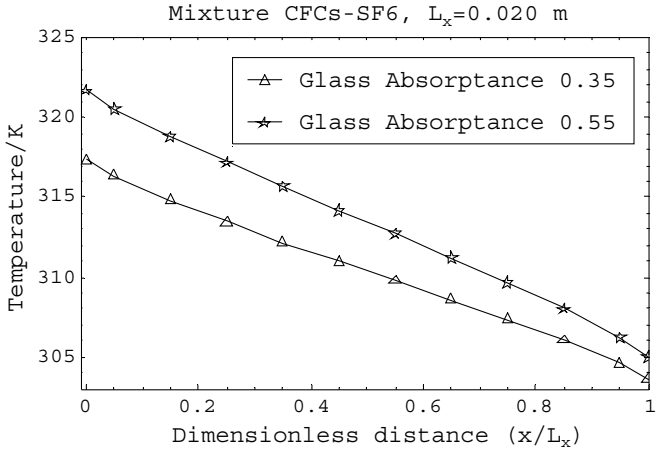

Fig. 11. Comparison of gas temperature distribution for different absorptance of external glass.

sheets having a gap filled with air. The results are shown in Fig. 12. One can observe that the coefficient of total heat gain, F, decreases slightly with the increase of the gap size. Also it is found that the highly absorbing gas mixture has higher F values, while the intermediate absorbing gas mixture has F values lying between strongly absorbing and transparent gas mixtures. The solar heat gain for double glass window with reflecting glass is lower than that of the clear glass case. Also, in Table 1b the coefficient of total

Table 1a
Non-gray radiation convection conduction modeling

L_x/m	Strongly (gas: HFCs-SF6) Absorbing glass	Medium (gas: CFCs-SF6) Absorbing glass	Transparent (gas: air) Absorbing glass	Air Clear glass
0.012	0.618335	0.587347	0.548799	0.887884
0.016	0.615753	0.580837	0.542190	0.887653
0.020	0.613004	0.570650	0.540863	0.887422
0.024	0.610534	0.567903	0.541727	0.887191
0.040	0.610058	0.567637	0.534492	0.886960

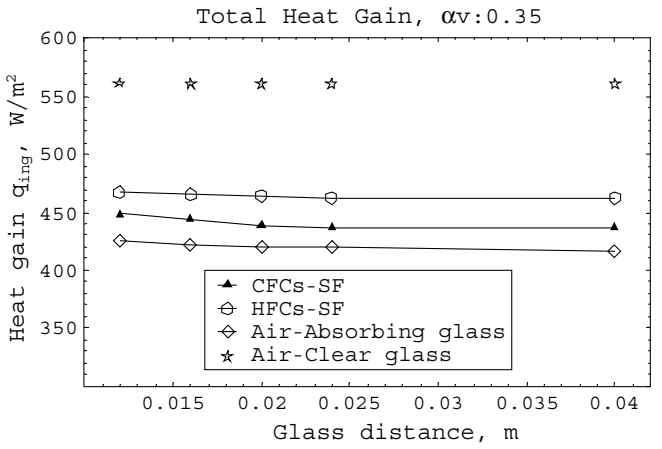

Fig. 12. Total heat gain coefficient.

Table 1b
Non-gray radiation conduction modeling

L_x/m	Strongly (gas: HFCs-SF6) Absorbing glass	Medium (gas: CFCs-SF6) Absorbing glass	Transparent (gas: air) Absorbing glass	Air Clear glass
0.012	0.606173	0.573476	0.555834	0.887884
0.016	0.603365	0.565394	0.547079	0.887653
0.020	0.597471	0.569761	0.541145	0.887422
0.024	0.590722	0.554156	0.536548	0.887191
0.040	0.579034	0.551522	0.526462	0.886960

heat gain F for $\alpha = 0.35$, in terms of the gap size for the three gas mixtures and the glass window filled with air for the pure radiative conductive model is presented. It is seen that the present radiative conductive conductive model predicts a slightly higher F values than the radiative conductive model.

Acknowledgments

The authors wish to thank the CNPQ for the financial support and the scholarships, for which the authors are highly indebted.

References

[1] H. Manz, Numerical simulation of heat transfer by natural convection in cavities of facade elements, Energy Build. 35 (2003) 305–311.
[2] J. Wright, A correlation to quantify convective heat transfer between vertical window glazings, ASHRAE Trans. 106 (1996) 940–946.
[3] S. Yin, T. Wung, K. Chen, Natural convection in an air layer enclosed within rectangular cavities, Int. J. Heat Mass Transfer 21 (1978) 307–315.
[4] EM 673, Glass in building: determination of thermal transmittance (U value), calculation method, European Committee for Standardization, Brussels, 1997.
[5] R. Miloni, V. Herrmann, Anti-reflective low E coated windows, Int. Glass Rev. 1 (200) (2000) 51–54.
[6] N. Wruk, Energy balance of coated double glazings, Glass Process. Days (September) (1997) 182–186.

[7] T. Eriksson, C. Granqvist, J. Karlsson, Transparent thermal insulation with infrared absorbing gases, Solar Energy Mater. 16 (1987) 243–253.
[8] S. Reilly, D. Arasteh, M. Rubin, The effects of infrared absorbing gasses on window heat transfer: a comparison of theory and experiment, Solar Energy Mater. 20 (1990) 277–288.
[9] K. Ismail, C. Salinas, Application of the CW model for the solution of non-gray coupled radiative conductive heat transfer in double glass window with a cavity filled with mixtures of absorbing gases, in: ICHMT International Symposium on Radiative Transfer—Radiation IV, Istanbul, 2004.
[10] T. Muneer, N. Abodahad, A. Gilchrist, Combined conduction convection, and radiation heat transfer model for double-glazed windows, Proc. CIBSE A 18 (4) (1997) 183–191.
[11] J. Taine, A. Soufiani, Gas IR radiative properties: from spectroscopic data to approximate modelsAdvances in Heat Transfer, vol. 33, Academic Press, San Diego, CA, 1999, pp. 295–414.
[12] M. Denison, B. Webb, A spectral-line based weighted-sum-of-gray-gases model for arbitrary RTE solvers, ASME J. Heat Transfer 115 (1993) 1004–1012.
[13] M. Modest, H. Zhang, The full-spectrum correlated-k distribution for thermal radiation from molecular gas-particulate mixtures, ASME J. Heat Transfer 124 (2002) 30–38.
[14] V. Solovjov, B. Webb, A local-spectrum correlated model for radiative transfer in non-uniform gas media, J. Quant. Spect. Radiative Transfer 73 (2002) 361–373.
[15] K. Ismail, C. Salinas, Application of local-spectrum correlated model to modeling radiative transfer in mixture of real gas media in bi-dimensional enclosures, Numer. Heat Transfer A 47 (2005) 183–207.
[16] L.S. Rothman et al., HAWKS (HITRAN Atmospheric Workstation): 1996 Edition, J. Quant. Spect. Radiative Transfer 60 (1998) 665–710.
[17] F. Incropera, D. DeWitt, Fundamentals of Heat and Mass Transfer, fourth ed., John Wiley and Sons, New York, 1996.
[18] R. Siegel, J.R. Howell, Thermal Radiation Heat Transfer, third ed., Washington, USA, 1992.
[19] W.A. Fiveland, Discrete ordinates solutions of the radiative transport equation for rectangular enclosures, Trans. ASME J. Heat Transfer 106 (1984) 699–706.
[20] K.A.R. Ismail, C. Salinas, Application of multidimensional scheme and the discrete ordinate method to radiative heat transfer in a two-dimensional enclosure with diffusely emitting and reflecting boundary walls, J. Quant. Spect. Radiative Transfer 88 (2004) 407–422.
[21] A.L. Crosbie, R.G. Schrenker, Radiative transfer in a two-dimensional rectangular medium exposed to diffuse radiation, J. Quant. Spect. Radiative Transfer 31 (4) (1984) 339–372.
[22] W. Yuen, E. Takara, Analysis of combined conductive–radiative heat transfer in a two-dimensional rectangular enclosure with a gray medium, ASME J. Heat Transfer 110 (1988) 468–474.
[23] R. Koch, R. Becker, Evaluation of quadrature schemes for the discrete ordinates method, J. Quant. Spect. Radiative Transfer 84 (2004) 423–435.